Dynamical polygonization below the cellular-bifurcation threshold in thin-sample directional solidification

Sabine Bottin-Rousseau,* Silvère Akamatsu, and Gabriel Faivre
Groupe de Physique des Solides, CNRS UMR 7588, Universités Denis-Diderot et Pierre-et-Marie-Curie, Tour 23, 2 place Jussieu, 75251 Paris Cedex 05, France
(Received 26 February 2002; revised manuscript received 12 April 2002; published 1 August 2002)

We show that a polygonization of the crystal (formation of grain subboundaries) takes place during the growth in thin-sample directional solidification of a transparent nonfaceted alloy at solidification rates lower than the cellular-bifurcation threshold. We give experimental evidence that this phenomenon is due to a dynamical coupling between the lattice defects intersecting the growth front and the diffusive modes of instability of the front. We present a theoretical model of this process in two-dimensional systems.

DOI: 10.1103/PhysRevB.66.054102 PACS number(s): 61.72.Mm, 47.54.+r, 81.10.Aj, 81.30.Fb

I. INTRODUCTION

In directional solidification, i.e., when solidification is performed at an imposed rate V under an externally applied unidirectional thermal gradient G, the growth front of a nonfaceted dilute alloy undergoes a morphological transition at a threshold value V_c of V: the front is planar (parallel to the isotherms) at $V<V_c$, and exhibits a periodically modulated (''cellular'') shape at $V>V_c$.[1] The physical factors at play are the solute concentration gradient ahead of the front, the applied thermal gradient, and the solid-liquid surface tension. The first exerts a destabilizing effect on the front, whereas the others tend to restabilize it. The exact nature of the transition (a bifurcation between different branches of stationary states of the system) was clarified by the linear theory of Mullins and Sekerka,[2] and subsequent weakly nonlinear analysis.[3] Experiments performed by the method of thin-sample directional solidification (TDS) of transparent alloys, in which the growth front was observed in real time with an optical microscope, were specifically dedicated to the checking of these theories, and fully confirmed their validity.[4]

However, some phenomena connected with the cellular transition remain unclear, for instance, the interplay between deformations of the growth front and crystal defects. The particular case of a high-angle grain boundary (GB) running perpendicular to the front was studied in some detail,[5,6] but little is known about the coupling of dislocations and grain subboundaries (SB's) with the movements of the front.[7] Some insight into this question was recently provided by Grange *et al.*[8] These authors visualized simultaneously the dislocations in the solid and the growth front during a directional solidification of metallic alloys using x-ray topography. They observed, among other things, that the crystals contained a relatively homogeneous dislocation network, which grew with the solid during solidification at $V<V_c$, and underwent rearrangements in response to the deformations of the front when V was switched to a value larger than V_c. Phenomena of this type are very likely to occur in all nonfaceted systems, especially, in the transparent organic ''analogs of metals,'' such as CBr_4 and succinonitrile, that are commonly utilized in TDS experiments.[9,10]

In this paper, we present an experimental study of a phenomenon, which, as we shall show, involves a rearrangement of the dislocations in the solid during solidification at $V<V_c$. This phenomenon, which was previously noted,[11] but not studied, consists of the repeated appearance of small grooves along the front. We study it here in detail in thin samples of the alloy CBr_4-C_2Cl_6, which, at low concentrations, solidifies into a fcc plastic crystal. Our purpose is twofold: first, we wish to illustrate the fact that relatively fine rearrangements of lattice defects can be easily, although indirectly, observed using an optical microscope; second, we try to utilize this fact to cast light upon the above-mentioned phenomenon, and thereby upon the elementary mechanisms through which deformations of the front associated with changes in the solute concentration field can be coupled with rearrangements of dislocations in the solid.

In recent years, the potential of the TDS method has been greatly increased by the use of powerful data processing techniques. Nowadays, this method allows one to follow a several-millimeter-wide portion of a front over a several-hour-long solidification time with a spatial sensitivity limit of less than 1 μm and a temporal resolution of 0.04 s. This technical progress played a decisive part in a recent clarification of old pending questions, such as the influence of interfacial anisotropy on the stability of cellular/dendritic patterns[12,13] and the nature of the morphological instabilities of lamellar eutectics.[14] The application of the TDS method that we present here relies on the following simple idea. The statement that the solidification front is planar when $V<V_c$ is true only if the solid is perfect. Any local accumulation of defects in the solid near the front increases the local free energy of the solid, lowers the solid-liquid equilibrium temperature, and hence creates a depression of the solidification front, which is potentially observable with an optical microscope. A well-known example is that of the grooves created by high-angle grain boundaries intersecting the front.[15] These GB grooves are several μm deep, generally. It is possible to observe much smaller deformations of the front. It will be seen that grooves no deeper than about 0.3 μm, attached to subboundaries of disorientation angles smaller than about 0.2°, can easily be vizualized.

The phenomenon that we study here can be briefly described as follows. A portion of a front, which was perfectly

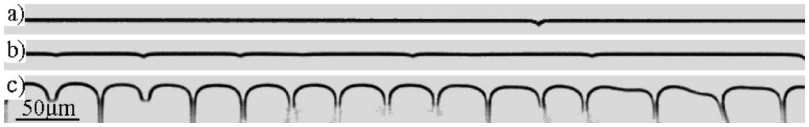

FIG. 1. Three snapshots of the same portion of a solidification front. Undoped CBr_4. $G=110$ K cm^{-1}. In this, and the following figures, the solidification direction is upward. (a) At rest ($V=0$) prior to solidification. The deep GB groove appearing in this snapshot is in the process of migrating rightward as a result of the grain coarsening process occurring in the solid. (b) After a 30-min solidification at $V=6.5$ μms^{-1}. Note the five shallow grooves that have appeared during solidification. The preexisting GB is still visible on the right-hand side of the photograph. (c) After a V jump to 20 μms^{-1}. The first and the third intercell grooves from the left are without SB's.

flat before the onset of directional solidification [Fig. 1(a)], exhibits a number of small grooves after a certain time of solidification at V substantially lower than V_c [Fig. 1(b)]. The existence of a cusp (visible at a larger magnification) at the bottom of these grooves, and the fact that they do not disappear when the solidification is stopped, indicate that they are attached to SB's. It is shown below that these SB's are the result of a ''dynamical polygonization,'' i.e., a rearrangement of the dislocation network occurring during growth.[7] Polygonization is commonly observed in ductile crystals at high temperature, but the puzzling fact here is that it occurs with a certain regularity during the whole duration of the solidification runs. Although the SB grooves are subject to a complicated dynamics, as will be seen, their average spacing remains fixed at a value of the order of magnitude of 100 μm. This value, which is comparable to the spacing of the large-amplitude cells appearing at $V>V_c$ [Fig. 1(c)], suggests that dynamical polygonization is a morphological instability precursory of the Mullins-Sekerka bifurcation. The study presented below essentially confirms the validity of this view, but also shows that the details of the process depend on the sample thickness, and several other geometric and crystallographic factors.

The existence of a dynamical polygonization below V_c is of some importance concerning the cellular bifurcation itself. When, after some time of pulling at $V<V_c$, V is switched to a value larger than V_c, either directly or after a stop of the solidification, the intercell grooves appear preferentially on the site of the shallow SB grooves created at $V<V_c$. Dynamical polygonization is thus responsible for a preselection of the intercell spacing. Furthermore, the existence of a SB intersecting the front near the bottom of an intercell groove modifies the shape of the groove [Fig. 1(c)]. The perturbation of the cellular pattern that this causes is generally, but not always, weak. For instance, it has been reported that, when the cellular pattern is close to the ''doublet'' bifurcation,[16] the presence of SB's attached to the intercell grooves plays a major role in the selection of the pattern.[17]

II. EXPERIMENTAL METHODS

Details about the used TDS setup and the material constants of the CBr_4-C_2Cl_6 alloy were given elsewhere.[12,13,18,19] The samples are made of two parallel glass plates separated by two thin plastic strips. The useful space is 9 mm wide, 60 mm long and 6, 12 or 50 μm thick. We take the thickness of the foils from which the plastic strips are cut up as the nominal value of the sample thickness. The difference between the actual sample thickness and this nominal value does not exceed a few μm. The observations show that the effects of this error may be quite significant in (nominally) 6-μm thick samples, but are generally negligible in 12- and 50-μm-thick ones. In this study, we preferentially use 12-μm-thick samples for reasons which will be explained later.

The alloys are prepared by mixing zone refined chemicals, but nevertheless contain a non-negligible amount of residual impurities. Two values of G (44 and 110 K cm^{-1}) and various values of the molar fractions C_∞ of C_2Cl_6 are used, but dynamical polygonization turns out to be qualitatively independent of C_∞ and G. The uncertainty on G is of about $\pm 10\%$. At $G=44$ K cm^{-1}, the measured values of V_c range from about 8 μms^{-1} in undoped CBr_4 samples (due to residual impurities) to 0.8 μms^{-1} for $C_\infty=8\%$.

The samples are filled by capillarity above the melting point of pure CBr_4 ($T_m\approx 92.5\,^\circ$C), cooled down to room temperature (the substance is then fully solidified) and sealed. They are then put between two ovens regulated at different temperatures, and maintained at rest (i.e., at $V=0$) during a certain time before the onset of the pulling. Their coldest end remains in the solid state, and serves as solidification seed. This seed is a polycrystal, as revealed by the presence of deep GB grooves at the solid-liquid interface, and is subject to a grain coarsening process.[20] We started the pulling after about 20 min at rest, at a moment when the grain size (i.e., the spacing of the GB grooves) was of about 500 μm. Between the GB grooves, the front was flat within experimental uncertainty [see Fig. 1(a)], any preexisting SB having been eliminated by the lateral migrations of the GB's during grain coarsening.

The stationary planar-front regime at $V<V_c$ is reached at the end of an initial ''solute redistribution'' transient,[21] during which the front recoils (in the reference frame of the laboratory) over the distance $l_{th}=\Delta T_o/G$ (thermal length), where ΔT_o is the difference between the temperature of the liquidus and that of the solidus at $C=C_\infty$. During this transient, the actual growth rate W of the front progressively increases from zero to V. Similarly, W decreases progressively from V to zero during the ''final'' transient following the arrest of the solidification. The characteristic time τ_D of these transients is equal D/V^2, where D (≈ 500 μm^2 s^{-1}) is the diffusion coefficient of C_2Cl_6 in liquid CBr_4.

At $V>V_c$, Mullins-Sekerka cells form during the initial transient. For reasons which we need not to give here, their actual spacing is generally significantly smaller than the theoretical value λ_c of the critical spacing.[22] To a good approxi-

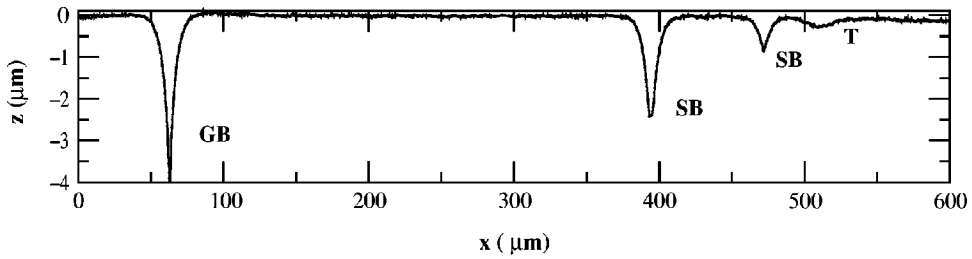

FIG. 2. Binarized profile of a solid-liquid interface after a 20-min stay at rest. $C_\infty = 1\%$. $G = 44$ K cm^{-1}. GB: high-angle grain boundary; SB: subboundaries; T: trough due to a smooth modulation of the dislocation density. The grooves have been truncated by the binarization procedure so that their apparent depth is smaller than their real one.

mation, the latter is given by $(\lambda_c/2\pi)^3 = 2d_o l_{th}^2/K$, where $d_o = a_o/\Delta T_o$ is the capillary length, $a_o = \gamma T_m/L_v$ (γ is the solid-liquid surface tension, and L_v is the latent heat per unit volume) is the Gibbs-Thomson capillary coefficient, K is the partition coefficient. In CBr_4-C_2Cl_6, $K \approx 0.75$ and $a_o \approx 0.086$ μmK.

During solidification, the growth front is continually observed with an optical microscope. The images are transferred to a tape recorder, and digitized for further analysis. Image processing was made with the public-domain NIH-Image software. Figure 2 shows the binarized profile of a front that has been maintained at rest for a certain time after a solidification run at $V < V_c$. In this and the following figures, the z axis is parallel to the growth direction, and the x axis to the isotherms. The y axis is normal to the plane of the sample. In Fig. 2, the profile has been stretched along the z axis by a factor of 20. Three types of distortions due to crystal defects can be seen, namely, a deep groove due to a GB, two shallower grooves of different depths due to two SB's of different surface tensions, and a rounded trough which is certainly due to a pronounced, but smooth maximum in the dislocation density, as will be seen below. The trough is clearly visible although it is only about 0.3 μm deep.

III. EXPERIMENTAL RESULTS

A. Shape of GB and SB grooves

The equilibrium shape of the GB grooves has been studied in a number of transparent and metallic nonfaceted systems with the aim of determining the solid-liquid surface tension.[23,24] The principle of the method is as follows.[15] The profile $\zeta(x)$ of a groove obeys the Gibbs-Thomson equation relating the temperature, the solute concentration, and the curvature of the front. When the concentration is uniform, the Gibbs-Thomson equation is entirely similar to the equation of a meniscus in a gravitation field. This equation is solved with the boundary condition that the slope $d\zeta/dx$ of the front at the junction with the GB is fixed by Young's equilibrium condition betwen the surface tensions. In the presence of capillary anisotropy, i.e., when the surface tensions depend on the orientations of the interfaces, Herring's version of the latter condition must be used. When the capillary anisotropy of the solid-liquid interface is negligible, which is the case in nonfaceted systems, the following formulas are obtained: let $\alpha_{GB} = \tan^{-1}(d\zeta/dx)$ be the pinning angle of the interface at the junction, h_{GB} the depth of the groove, and γ_{GB} the surface tension of the boundary; these quantities are related to each other by $\gamma_{GB}/\gamma = 2 \sin \alpha_{GB}$ and $h_{GB} = \sqrt{2} d_m \sin(\alpha_{GB}/2)$, where $d_m = \sqrt{2 a_o / G}$ is the meniscus length. In the case of SB's, these relations read

$$\alpha_{SB} \approx \gamma_{SB}/2\gamma \approx \sqrt{2} h_{GB}/d_m . \tag{1}$$

Furthermore, SB's fulfill the condition $\gamma_{SB} < 2\gamma$ and GB's the condition $\gamma_{GB} = 2\gamma$ near T_m. The latter condition, which we shall regard as a definition of the GB's valid near T_m, means, roughly speaking, that GB's are wetted by the liquid. Consequently, all GB's have the same groove depth d_m, while SB's have groove depths smaller than d_m. Furthermore, the capillary anisotropy of the GB's is small, like that of the solid-liquid interface, whereas that of the SB's is generally strong. Consequently, in equilibrium, GB's cut the front at a right angle, whereas SB's may intersect it at an angle substantially different from 90°.

We have observed these distinctive features of the GB and SB grooves in our system. In this section, we focus on the shape of the grooves themselves, which does not depend on the capillary anisotropy of the grain boundaries. The pinning angles and depths of the grooves were determined by fitting the theoretical formula for a semi-infinite meniscus onto the well-resolved part of the profiles. For the deepest grooves, we found $d_m = 6.3 \pm 0.4$ μm for $G = 44$ K cm^{-1}, corresponding to $\gamma = 8.7 \pm 1$ mN m^{-1}, in good agreement with previous measurements.[18] For the SB's, the measured values of h_{SB} ranged from 0.3 μm to d_m. Incidentally, we have considered the possibility that the grooves created during growth, or, at least, some of them, be due to tiny dust particles floating in the liquid.[25] In fact, we observe, occasionally, small troughs due to particles of a size of 1 μm or so, which are pushed along by the front during a certain time before being engulfed by the solid, but these troughs are rounded, and moreover nonstationary because of the incessant motions of the particle in the liquid. More decisively, they disappear in a few seconds when the pulling is stopped. Thus no confusion between a groove due to a SB and a trough due to a particle seems possible.

The order of magnitude of the surface tension of a subboundary is given as a function of the disorientation angle θ_{SB} by the well-known Read-Shockley formula, which reads

$$\gamma = \gamma_m \theta_{SB}/\theta_m [1 - Ln(\theta_{SB}/\theta_m)], \tag{2}$$

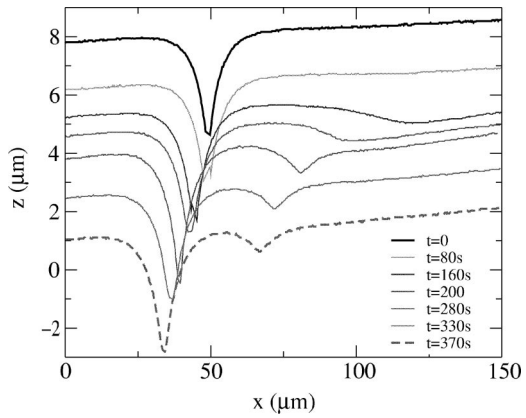

FIG. 3. Profiles of a solidification front near a GB at the indicated times. Pulling was started at 2.15 μms^{-1} at $t=10$ s. The successive profiles have been shifted downwards by arbitrary quantities. $C_\infty=1\%$. $G=44$ K cm^{-1}.

where γ_m and θ_m are semiempirical material constants.[7] In fcc crystals, θ_m is close to 30° and $G_e b/\gamma$, which is closely connected to the ratio of the energy of cohesion to the latent heat of melting, is of about 50.[26] Using these estimates, we found $\theta_{SB}\approx 0.2°$ for $h_{SB}=0.3$ μm. The corresponding value of the pinning angle is $\alpha_{SB}\approx 4°$. To a good approximation, the function of θ on the right-hand side of Eq. (2) can be replaced by a linear function over a wide interval around 0.2°. If the actual value of $G_e b/\gamma$ in our system turned out to be, say, twice as large (small) as the above estimate, the estimated value of θ_{SB} for $h_{SB}=0.3$ μm would be divided (multiplied) by 2.

The order of magnitude of the inter-dislocation spacing in a SB is of b/θ_{SB}. In CBr_4, $b=\frac{1}{2}\langle 110\rangle\approx 0.63$ nm. Thus a SB with a groove depth of, say, 0.3 μm corresponds to about 50 dislocations piled up in the thickness of a 12-μm-thick sample. The dislocation density n_d corresponding to a periodic array of SB's of spacing l_o is given by

$$n_d \approx \frac{\theta_{SB}}{b l_o}. \tag{3}$$

In our case, $l_o>50$ μm and $h_{SB}\approx 1$ μm. Thus the dislocation density contained in the dynamically created SB's at a given pulling time is at most of 5×10^3 cm^{-2}. A dislocation density of this order of magnitude is usually found in as–grown crystals, and most probably exists already in the seed. Whether or not this suffices to feed the observed polygonization process will be discussed later.

B. Process of formation of the SB's

Figure 3 shows the shape of the interface at different stages of the process of creation of a SB in the vicinity of a preexisting GB in a 12-μm-thick sample. It is seen that a smooth depression appears at a relatively large distance $l \approx 80$ μm from the GB groove, and grows progressively deeper until it suddenly transforms into a cusp-shaped groove, indicating that a SB has been created in the solid. This occurs at the time $\tau\approx 150$ s from the onset of solidification. A lateral drift of the SB groove, due to the surface tension anisotropy of the SB, should also be noted. A drift of the GB groove is also apparent, but it is due to the above-mentioned grain coarsening occurring in the solid, and is of no importance here.

In other experiments, the solidification was intentionally stopped at different stages of the process. It was observed that, when the solidification is stopped a few seconds after the appearance of a depression, a complete recovery of the planarity of the front is observed, whereas a stable rounded trough remains at the front when the solidification is stopped a short time before the expected appearance of a cusp (this is the origin of the trough T in Fig. 2). This indicates the nature of the considered process: a depression exists before any significant rearrangement of the dislocations has taken place; this depression deepens, and becomes a well-localized trough as dislocations accumulate in it. The process ends by the ''nucleation'' of a SB at the point where the dislocation density is the highest—probably when this density first reaches some threshold value. We also note that $\tau_D\approx 108$ s and $\lambda_c\approx 105$ μm in the experiment of Fig. 3. Thus the characteristic quantities τ and l of the process are comparable to those of the diffusive dynamics of the front.

Figure 4 shows a spatiotemporal diagram obtained by superposing binarized low-magnification snapshots taken at regular time intervals δt and shifted along the growth axis by the length $V\delta t$. Such a diagram displays the history of a portion of the front in the reference frame attached to the solid. In Fig. 4, the rectilinear portions of the front have been erased in order to make the trajectories of the SB and GB grooves appear more clearly. Several upward V jumps were applied during this particular run. The last value of V was larger than V_c. It can be seen that, at $V<V_c$, the trajectories of the SB's form a river pattern. The SB's never appear by pairs, as they would if they were due to the nucleation of disoriented crystals. Three categories of events are observed: creations of SB's at some distance of preexisting GB's or SB's, mergings of two SB's, and abrupt changes in the lateral drift velocity of the SB's that are apparently not connected with mergings of SB's. We have not detected any significant difference between patterns formed in different grains, nor any global trend concerning the disorientation of the created SB's. In a few cases, the merging of a certain number of dynamically created SB's eventually gave rise to a GB, but this was probably a matter of statistical fluctuation.

The central fact revealed by the spatiotemporal diagrams is that dynamically created SB's act as sites for the creation of further SB's in the same way as preexisting GB's do. The mechanism through which polygonization propagates along the front is thus obvious. It strongly suggests that the planar front is actually linearly unstable against dynamical polygonization. A further indication of this is given by the sets of three or more equidistant grooves, which appear in the profiles of the front when the lateral drift of the SB's is not very fast (see Figs. 2 and 5 near $x=450$ μm). These configurations are similar to (although much less ample than) those that transitorily appear near the GB grooves at V slightly larger than V_c when Mullins-Sekerka cells begin to form along an unstable planar front.[11]

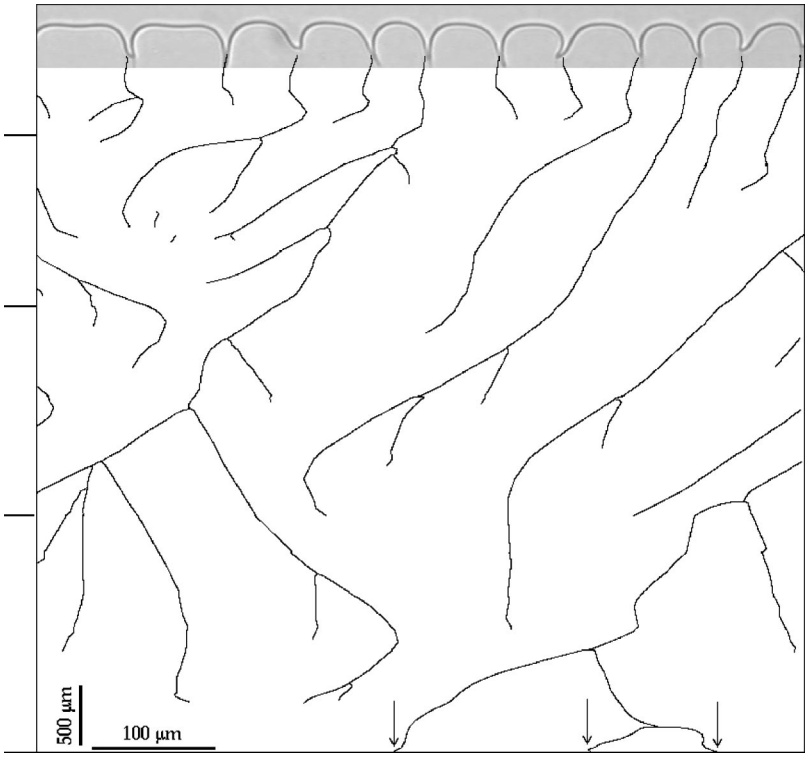

FIG. 4. Trajectories of the SB and GB grooves during a run performed at several different values of V. $C_\infty = 8\%$. $G = 110\ \mathrm{K\,cm^{-1}}$. Tick marks on the left-hand side indicate changes of V. The successive values of V are 1.8, 2.15, 2.8, and 3.8 $\mu\mathrm{ms}^{-1}$. The last value of V is above V_c. Arrows: preexisting GB's. Top: nonprocessed snapshot of the front (the vertical scale is equal to the horizontal one).

Quantitatively, the local features of the river pattern do not vary with time at fixed V. They are also practically independent of V, except when V approaches V_c. It can be seen in Figure 4 that the characteristic quantities l (distance between creation sites and preexisting grooves) and τ (lifetime of segments of the front longer than $2l$) kept the same order of magnitude until V was switched to a value larger than V_c. The sudden decrease of l and τ which was then observed will be considered later.

C. Lateral drift of the SB grooves

The orientation of the SB's in the solid is revealed by two faint dark lines running along their intersections with the solid-glass interfaces.[27] These lines are due to shallow liquid channels, which appear during solidification and subsist a certain time after the stopping of the pulling. We have observed that, contrary to GB's, SB's are often tilted with respect to both the growth axis and the glass plates. The proportion of SB's which are tilted with respect to the glass plates increases with increasing sample thickness. In 12-μm-thick samples, most of them are perpendicular to the glass plates, as revealed by the fact that they leave behind a single dark line in the solid (Figs. 6 and 7).

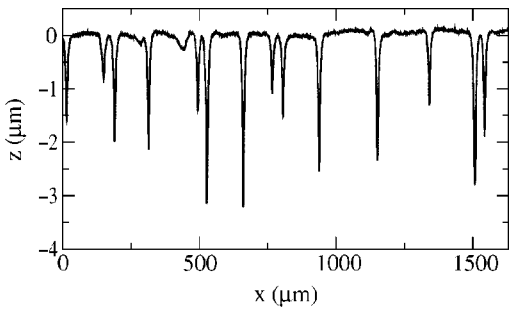

FIG. 5. Profile of the same front as in Fig. 3 at rest after a 10-min pulling at 2.15 $\mu\mathrm{ms}^{-1}$.

Figure 6 shows a snapshot of a drifting SB groove superimposed onto its spatiotemporal diagram. The dark line behind the groove coincides with its trajectory, indicating that the SB remained immobile in the solid during solidification. It did not change orientation when the pulling was stopped. The complete immobility of the SB's in the solid is also illustrated in Fig. 7, where the SB's obviously have out-of-equilibrium shapes. Thus the observed drift of the SB grooves is only due to the tilt of the SB planes with respect to the growth axis, which is itself due to the capillary anisot-

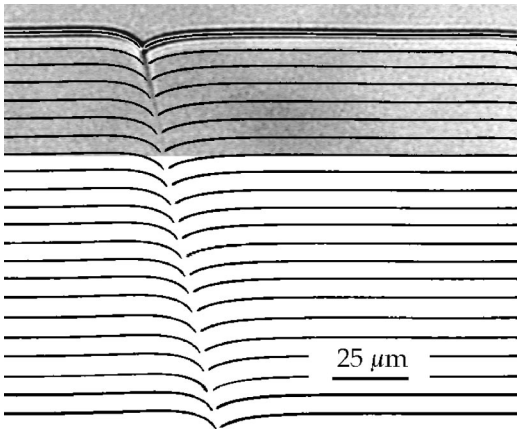

FIG. 6. Spatiotemporal diagram of a front near a SB groove. $V = 3.44\ \mu\mathrm{ms}^{-1}$. $C_\infty = 1\%$. $G = 110\ \mathrm{K\,cm^{-1}}$. The time interval between the snapshots is of 44 s. Top: nonbinarized snapshot of the front.

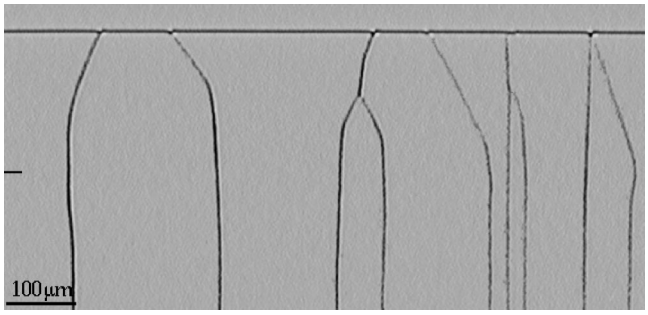

FIG. 7. SB's left behind in the solid after the stopping of a pulling at 20 μms^{-1} . Undoped CBr_4. $G=44$ K cm^{-1}. Tick mark: position of the growth front when the pulling was stopped.

ropy of the SB's, as explained in Sec. III A. This implies that the drift velocity V_{drift} of the groove and the tilt angle ϕ of the plane are related by the equation $V_{drift}=V\tan\phi$.

The low mobility of the SB's in the solid also implies that the observed SB planes only are materializations of the trajectories of the junction lines. In other words, these trajectories are determined by the sole condition that the Young-Herring law is fulfilled at the junctions during growth, whether the SB's left behind in the solid fulfill the equilibrium (Wulff's) condition in the solid or not. We have calculated the stationary profile and tilt angle ϕ_{st} of a weakly anisotropic SB groove as a function of V in the linear (or small pinning angles) approximation formerly used by Coriell and Sekerka. This calculation is not reproduced here. We find that, roughly speaking, ϕ_{st} is practically independent of V (and thus equals the Young-Herring equilibrium value at rest) when V is lower than a certain value close to V_c, and decreases rapidly with increasing V above this value. This result is in qualitative agreement with the observations, as illustrated in Fig. 7. This figure shows the trajectories of SB's during the final transient of a run performed at $V>V_c$. It can be seen that the tilt angle of the trajectories, which is practically equal to zero during the pulling, took a finite value at the beginning the transient, and then kept this value until the front came to rest. This may be explained on the basis of the above calculation by assuming that, during the final transient, i.e., during the decrease of the growth rate W from V to zero, the instantaneous values of the tilt angles of the SB's were equal, or were close to $\phi_{st}[W(t)]$.

This conclusion (V_{drift} is fixed by the anisotropy of γ_{SB}) implies that the drift velocity of a SB cannot change without the nature of the SB's, i.e., the orientation of the adjacent grains, changing. This in turn cannot occur without a merging of the considered SB and another SB. However, abrupt changes of V_{drift}, which are not connected with collisions between SB's, are often observed in the spatiotemporal diagrams (Fig. 4). A closer examination of the experiments from which the spatiotemporal diagrams originate provides a solution to this apparent contradiction. Figure 8 shows the profile of a front near a SB, which is in the process of changing its growth direction. The SB groove is in fact colliding with a rounded trough, which is too shallow to appear in the spatiotemporal diagram. Most probably, this trough is due to a group of dislocations equivalent to a SB, i.e., carrying a finite long-range disorientation of the crystal lattice, so that its incorporation into the SB changes the nature of the latter. Most of the irregularities in the trajectories of the SB's are likely to be due to similar processes, although the reverse process (a SB losing some of its dislocations) is also conceivable.

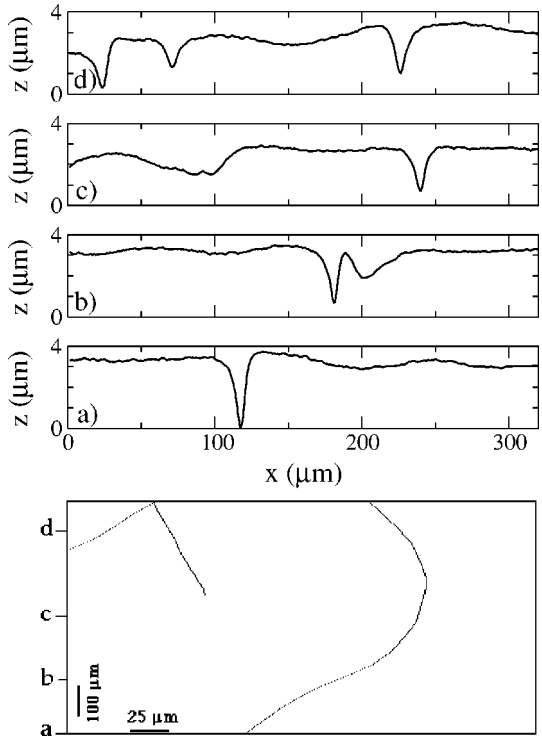

FIG. 8. Collision of a SB groove with a rounded trough. Below: spatiotemporal diagram. Above: binarized snapshots taken at the times indicated by the tick marks on the left-hand side of the spatiotemporal diagram. $V=1.85$ μms^{-1}. $C=8\%$. $G=110$ K cm^{-1}.

These remarks raise a question about the origin of the dislocations feeding the polygonization process. As mentioned, the total number of dislocations involved in the process is not large, and could well already be contained in the seed. However, spatiotemporal diagrams show that a region of the crystal, which has been swept by SB's (or GB's) several times, still contains a sufficient density of dislocations for SB's to be created. This persistent dislocation density is either left behind by the drifting boundaries or generated by some unknown mechanisms. Thermal stresses[28] or dust particles[25] either floating in the liquid or sticked on the glass plates, might be involved in these mechanisms, but this is not supported by our observations. Thermal stresses, if they were important, would presumably cause a noticeable plastic deformation of the solid at some distance behind the front.[29] Signs of the large increase in the dislocation density that such a deformation, if any, would cause, should appear during directional remelting of the samples,[30] but we observed none. In fact, the directional-remelting spatiotemporal diagrams revealed exactly the same SB patterns as the antecedent directional-solidification diagrams did. Thus, without surprise, our study leaves the question of the multiplication of

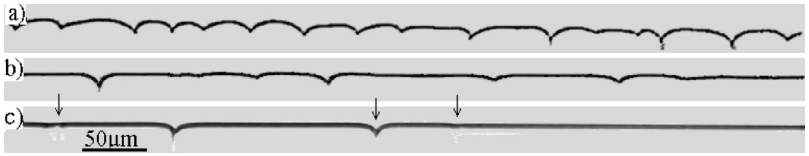

FIG. 9. Solidification fronts after a long time of pulling in three samples of different thicknesses. Sample thickness: (a) 6 μm, (b) 12 μm, and (c) 50 μm. In (c), the dynamically created SB grooves are indicated with arrows. Two of them are hardly visible because they correspond to SB's that are strongly tilted with respect to the glass plates. $V=2.8\ \mu\mathrm{ms}^{-1}$. $C=8\%$. $G=110\ \mathrm{K\,cm}^{-1}$.

the dislocations during growth open. Fortunately, this is unimportant as regards the qualitative nature of the polygonization process.

D. Three-dimensional effects. Influence of the sample thickness

Up to this point, we have implicitly assumed that the dynamics of our system was purely two dimensional (2D), i.e., that everything in the system, especially, the shape of the front, was uniform in the direction normal to the glass plates. In the remainder of this section, we consider processes that obviously violate this condition. It should be noted first that the growth front is actually nonplanar at $V<V_c$ even in the absence of lattice defects because it is in contact with the walls of the container, and thus forms a meniscus in the y direction. There is evidence that, in our system, the liquid wets the glass plates completely, i.e., that the pinning angle of the front at the glass plates is of 90°. Thus the front forms two grooves of characteristic width d_m along the junction line with the glass plates. This explains that the optimum value of the sample thickness for the observation of a quasi-2D dynamics is of the order of magnitude of $2d_m$ ($\approx$12 μm in our case).[12–14,19] In much thicker samples the dynamics of the system is intrinsically 3D, while in much thinner ones it is perturbed by a strong meniscus effect, and by the ''noise'' due to the irregularities of the glass plates. It should be noted that some processes involve only lengths smaller than d_m, and occur at whatever sample thickness. This is the case of the above-mentioned liquid channels running along the junction lines of the SB's with the glass plates.

Figure 9 shows typical front profiles observed in samples of different thicknesses solidified in otherwise similar conditions. It is seen that the average number of visible SB's decreases with increasing sample thickness. The proportion of SB's that are tilted with respect to the glass plates, and are therefore difficult to detect in the micrographs, increases with increasing sample thickness, as already mentioned. This effect is certainly partly responsible for the apparently smaller density of SB's in 50-μm-thick samples than in 12-μm-thick samples. Another important effect is connected with the 3D character of the SB nucleation process. The characteristic length of this process inside the solid (b/θ_{SB}) is microscopic, but it is associated with the creation of liquid channels along the glass plates, which is observable with an optical microscope. Figure 10 shows that the nucleation of a SB is often preceded by an oscillation, indicating that the configuration existing at the bottom of the rounded troughs is metastable against SB nucleation. Concerning the physical origin of this effect, we are reduced to conjectures. It might be due to the fact that the dislocations actually accumulate near the walls of the container, more precisely, at the intersections of the thalwegs of the troughs with the walls of the container. The x-ray topography observations by Grange *et al.*,[8] showing that the dislocations always emerge from the solid at points located relatively far behind the foremost point of the front, lend support to this view. The creation of a SB would then involve a propagation from a nucleation site located near a glass plate, and would be more difficult in thick, than in thin samples.

The large increase of the number of visible SB's in the (nominally) 6-μm-thick samples cannot be explained by the above two effects. In fact, the average spacing of the GB's is clearly smaller than λ_c in these samples, while the above effects can only result in a spacing larger than this value, if the conclusions of Sec. III B are correct. The theoretical model explained below suggests a solution to this apparent inconsistency. According to this model, at $V<V_c$, the observed distribution of SB's should reflect the structure of the predominant external perturbations. The observed difference in SB spacing between 12- and 6-μm-thick samples could thus originate from the fact that the predominant perturbation is the Coriell-Sekerka deformation associated to GB's (see below) in the former case, and the irregularities of the glass plates in the latter case, but this is not proven. Further studies in samples of very small, accurately controlled thicknesses will be necessary to clarify this point.

IV. A TWO-DIMENSIONAL MODEL

Coriell and Sekerka showed theoretically that the first Mullins-Sekerka cells appearing near the GB grooves when

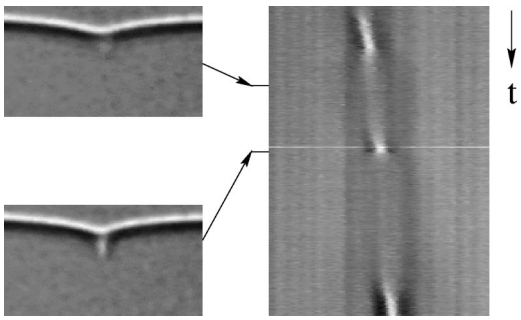

FIG. 10. Oscillations preceding the nucleation of a SB. Right: spatiotemporal diagram. Left: snapshots of the front at the times indicated by the tick marks. The width of the field of view is of 140 μm. The duration of the recording is of 8.3 s. $V=2.15\ \mu\mathrm{ms}^{-1}$. $C=8\%$. $G=110\ \mathrm{K\,cm}^{-1}$.

V is switched to a value larger than V_c result from the amplification of a long-range deformation of the front existing already at $V<V_c$.[5] This deformation is the response of the ideal (dislocation-free) system to the presence of a GB groove. The long-range tail of the deformation has the form of a damped sinusoid, the wavelength of which depends on V (it increases from d_m to λ_c when V increases from 0 to V_c), but is comparable to λ_c when V is larger than about $0.5V_c$. The amplitude of the sinusoid also increases as V increases, but remains very small until V reaches V_c.

We suppose that the smooth depression of the front appearing during the early stages of the process of creation of SB's (Fig. 3) is the first mimimum of the Coriell-Sekerka damped sinusoid attached to the nearby GB or SB groove. This assumption is quite compatible with the observed values of l and τ, and is supported by the fact that this depression relaxes completely when the solidification is stopped. In order to explain the subsequent amplification of the depression, it obviously suffices to assume that the dislocations of the solid are subject to a dynamical constraint, which drives them toward the bottom of whatever depression exists along the front. These assumptions can be put in the form of a 2D continuous model. In this model, individual dislocations are replaced by ''elementary'' SB's (ESB's) of an arbitrarily small disorientation α_e oriented perpendicular to the glass plates and the growth front (the anisotropy of the surface tension is neglected), and immobile in the solid. The distribution of the ESB's is described by a continuous density $l^{-1}(x,t)$. The other assumptions of the model are those that are usually made in the study of diffusive growth (no diffusion in the solid, infinitely fast interfacial kinetics, no anisotropy of γ, no convection in the liquid, linear temperature distribution imposed from the outside). The aim is to perform a linear stability analysis of the planar stationary states of this model. We shall content ourselves with an outline of the calculation.[22]

The unknown functions are three in number: the concentration field $C(x,z,t)$ in the liquid, the profile $\zeta(x,t)$ of the interface, and $l(x,t)$. In the stationary states, the front is at a fixed position ζ_o, the ESB spacing has a uniform value l_o, and the concentration field is given by $C_o(x,z)=(K^{-1}-1)C_\infty \exp[-(z-\zeta_o)l_D^{-1}]+C_\infty$, where $l_D=D/V$. The infinitesimal perturbation to be added to this state reads

$$\delta C = C_k e^{-qz} e^{ikx+\omega t},$$

$$\delta \zeta = \zeta_k e^{ikx+\omega t}, \tag{4}$$

$$\delta l = l_k e^{ikx+\omega t},$$

where k and ω are the wave vector and the amplification coefficient of the perturbation, respectively, C_k, ζ_k and l_k are unknown coefficients, and $ql_D=1/2+\sqrt{1/4+k^2l_D^2+\tau_D\omega}$. It is assumed that $\Lambda \gg l_o$, where $\Lambda=2\pi/k$. The object of the calculation is to find the stability spectrum $\omega(\Lambda)$ at fixed values of the other parameters. The planar front is unstable if there exists a range of Λ in which $\omega(\Lambda)>0$. It is understood that the growth of the unstable modes will end by the collapse of the ESB's into SB's of a finite disorientation in the regions corresponding to the minima of $\zeta(x)$ [i.e., it will lead to a regular polygonization array], but this is not included in the mathematical model.

We need three independent equations at the solid-liquid interface for the three unknown functions. Two equations—namely, the mass conservation and the Gibbs-Thomson equations—are provided by the standard model. A third equation must impose that the ESB's draw nearer to the minima of $\zeta(x)$ during growth. In fact, this condition is implicitly contained in our model since the equilibrium conditions at the junctions impose that SB's grow perpendicular to the local orientation of the front. A similar rule, called Cahn's hypothesis, has been conjectured long ago for the interphase boundaries in lamellar eutectic growth, and it is well known that it leads to an accumulation of the defects in the troughs of the front.[31] The equation that expresses this constraint reads[32]

$$\frac{\partial l}{\partial t} + l_o V \frac{\partial^2 \zeta}{\partial x^2} = 0. \tag{5}$$

It should also be noted that ESB's of pinning angles α_e and spacing l impose an average curvature $2\alpha_e l^{-1}$ to the front. Thus the coupling between the lattice defects and the front appears in the form of an additional term $\Delta T_e(x)=-2a_o\alpha_e l^{-1}(x)$ on the right-hand side of the Gibbs-Thomson equation.

The thus-defined model is basically similar to the continuous Langer-Cahn model of lamellar eutectics.[32–34] In the latter model, we recall, the defects responsible for the curvature term ΔT_e are the boundaries separating the two solid phases. It was shown long ago that, if this term is acting alone, and if Cahn's hypothesis is valid, the front is unstable against any long-wavelength perturbation (long meaning much larger than l).[31] The mechanism of this instability is as follows. Suppose that, for some reason, a trough appears along the front. Cahn's hypothesis implies that the defects will accumulate into this trough. The curvature term will thus become larger inside the trough, i.e., the trough will deepen, which will in turn accelerate the accumulation of the defects into the trough. In the case of lamellar eutectics, ΔT_e is counteracted by a solutal term, which stabilizes the front above a certain ''minimum-undercooling spacing.'' Such a term does not exist in the present model, so that it is clear, prior to any calculation, that the stationary planar state of our model is unstable for any value of V. The following calculation permits to specify the nature of the fastest growing mode, and the variation of its amplification rate as a function of V.

Injecting the perturbed solution into the interface equations, and linearizing with respect to the perturbative terms, one obtains a homogeneous linear system for C_k, ζ_k, and l_k, the secular equation of which gives the following implicit equation for ω,

$$\tau_D\omega^2 - \omega[(1-V_{cs}V^{-1}-d_o l_D k^2)(ql_D-1+K)-K] - \beta_e D k^2 (ql_D-1+K)=0, \tag{6}$$

where $V_{cs}=D/l_{th}$ is the ''constitutional-supercooling'' threshold velocity,[21] and $\beta_e=2\alpha_e d_o l_o^{-1}$ is a dimensionless

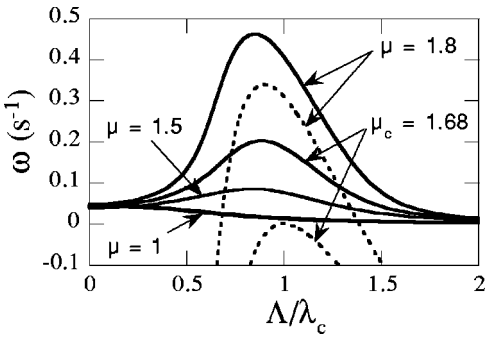

FIG. 11. Calculated stability spectra for the indicated values of $\mu = V/V_{cs}$. The values of the other parameters are given in the text. The Mullins-Sekerka threshold corresponds to $\mu = 1.68$. Continuous lines: with lattice defects ($\beta_e = 4 \times 10^{-4}$). Broken lines: without lattice defects ($\beta_e = 0$).

parameter. Note that the arbitrary parameters l_o and α_e appear only through their ratio, which is approximately proportional to the dislocation density n_d. In fact, $\beta_e = 2Cn_d b d_o$ [see Eq. (3)], where $C = \theta_e / \alpha_e$ is approximately constant in the range of interest. Also note that one obtains the usual Mullins-Sekerka stability equation by setting β_e to zero in Eq. (6).

Figure 11 shows the stability spectrum $\omega(\Lambda)$ calculated for various values of V and the indicated values of the parameters. The curves $\omega^{(p)}(\Lambda)$ for an ideal crystal ($\beta_e = 0$) are shown for comparison. The values of d_o ($= 0.32$ μm), and the other parameters are those of CBr_4-C_2Cl_6 for $C_\infty = 0.01$ and $G = 110$ K cm^{-1}. For this set of parameters, the roots of Eq. (6) are real near the critical point as is also the case in the underlying Mullins-Sekerka model.[3] Only the largest of the roots appears in Fig. 11. The value taken for β_e (4×10^{-4}) corresponds to $n_d \approx 5 \times 10^6$ cm^{-2}. This value, which is probably much above the actual value of n_d in our samples (see above), was chosen for the sake of clarity.

It can be seen that ω is positive for any value of Λ and V, as expected, but that a qualitative change occurs at $V = V_{cs}$. Below V_{cs}, $\omega(\Lambda)$ is a monotonic function which decreases from $\omega_o = \beta_e V / d_o$ for $\Lambda \to 0$ to zero for $\Lambda \to \infty$. We note that $1/\omega_o$ is large compared to the usual duration times of solidification runs for realistic values of β_e. On the other hand, a maximum appears at a finite wavelength Λ_{fst} (where "fst" stands for "fastest growing mode") at $V = V_{cs}$. The maximum value ω_{fst} of the amplification rate increases with increasing V. At V_c (i.e., at the value of V at which, in the absence of defects, ω_{fst}^{-1} would be infinitely large), ω_{fst}^{-1} is of about 1 s, thus very small compared to experimental duration times. The reason for this change occuring at V_{cs} is as follows. In the absence of lattice defects, the stability of the planar front within the range $V_{cs} < V < V_c$ is due to capillary forces, i.e., to the negative term proportional to d_o appearing in Eq. (6) (note that $q l_D \gg 1$ in the range of Λ of interest). The presence of defects that are forced to grow normal to the front introduces a positive capillary term, which destroys the usual stabilizing effect of the surface tension.

Before comparing these theoretical results with the experimental observations, we emphasize again that the morphological transition described by the model at $V < V_c$ (the dynamical polygonization) is essentially different from the cellular transition occurring at V_c. Dynamical polygonization consists of a rearrangement of a limited number of dislocations (n_d) initially present in the crystal. It stops when all the dislocations have collapsed into subgrain boundaries. It is true that the front eventually takes on a "precellular" aspect [Figs. 1(b) and 9], but the amplitude of the "precells," which is nothing else than the depth of the SB grooves, is bounded and essentially independent of V [Eqs. (1) and (3)]. This polygonized front destabilizes at V_c, giving rise to Mullins-Sekerka cells.[5,6] Above V_c, the amplitude of the cells is hardly affected by the presence of a polygonization.

It must also be emphasized that the observed behavior of a front depends not only on the instability spectrum but also on the perturbations to which it is submitted. Some potentially important sources of noise in our samples (wall effects, intrinsic fluctuations of the dislocation density) are ill known, which forbids a really quantitative comparison between models and experiments. However, the following semiquantitative predictions can be made:

(1) For $V < V_{cs}$, a destabilization will only be observed in the regions where an ample external deformation (as, for instance, a GB groove) is imposed to the front. Because of the flatness of the spectrum, this localized deformation will first amplify keeping an unchanged shape, and then propagate along the front.

(2) for $V_{cs} < V < V_c$, any small perturbation will suffice to trigger a deformation of the front, which will tend to become a periodic modulation of wavelength Λ_{fst} whatever its initial shape.

The first of these predictions is in agreement with the numerous well-reproducible observations made in 12-μm-thick samples at V substantially lower than V_c (Sec. III A). It may also explain the difference in SB spacing between 12- and 6-μm-thick samples at $V < V_{cs}$ via the wall effects, as explained in Sec. III D. The second prediction is in agreement with the rapid appearance of more or less equispaced SB grooves that we observed to occur in response to V jumps from a velocity lower, to a velocity higher than V_c (Fig. 4).

V. CONCLUSION

We have brought to light a mechanism coupling the dislocations intersecting the solidification front of a nonfaceted crystal with the long-range diffusive deformations of this front. This mechanism leads to a regular polygonization of the crystal during directional solidification at $V < V_c$ in 2D systems. Furthermore, we have shown that the observed lateral drift of the junctions of the dynamically created SB's with the front can be explained by the surface tension anisotropy of the SB's. These two ingredients could serve as a basis for a 2D model, which, most probably, could explain all the observations that we have made in 12-μm-thick samples. An important experimental fact would however escape such a model, namely, the sensitivity of dynamical

polygonization to sample thickness. We have attributed this sensitivity to the fact (proven in former studies) that our system is quasi-2D only in a relatively narrow sample thickness window around 12 μm. Since solidification is generally performed in samples much thicker than this value, the most interesting question opened by this study is that of the polygonization dynamics in 3D systems. The only, relatively obvious, prediction that can be made at present is that dynamical polygonization is certainly more complex, less regular, and globally less effective in thick than in thin samples because, in thick samples, the dynamically created SB's are not constrained to be perpendicular to the walls. Consequently, they generally intersect, and merge into the preexisting high-angle grain boundaries. Real-time observations of the growth front of thick samples are currently in progress in order to clarify this question.

ACKNOWLEDGMENT

This research was financially supported by the Centre National d'Etudes Spatiales, France.

*Electronic address: bottin@gps.jussieu.fr

[1] J.W. Rutter and B. Chalmers, Can. J. Phys. **31**, 15 (1953).
[2] W.W. Mullins and R.F. Sekerka, J. Appl. Phys. **35**, 444 (1964).
[3] D.J. Wollkind and L.A. Segel, Philos. Trans. R. Soc. London, Ser. A **268a**, 351 (1970); B. Caroli, C. Caroli, and B. Roulet, J. Phys. (Paris) **43**, 1767 (1982).
[4] W. Losert, B.Q. Shi, and H.Z. Cummins, Proc. Natl. Acad. Sci. U.S.A. **95**, 431 (1998).
[5] S.R. Coriell and R.F. Sekerka, J. Cryst. Growth **19**, 285 (1973).
[6] L.H. Ungar and R.A. Brown, Phys. Rev. B **30**, 3993 (1984).
[7] For an introduction to the physics of lattice defects, see D. Hull, *Introduction to Dislocations* (Pergamon Press, Oxford, 1975). Subboundaries (or low-angle grain boundaries) are made of two-dimensional periodic arrays of dislocations devoid of long-range stresses. Polygonization is the generic name of the rearrangement processes giving rise to subboundaries.
[8] G. Grange, C. Jourdan, J. Gastaldi, and B. Billia, J. Phys. III **4**, 293 (1994).
[9] K.A. Jackson and J.D. Hunt, Acta Metall. **13**, 1212 (1965).
[10] H.M. Hawthorne and J.N. Sherwood, Trans. Faraday Soc. **66**, 1783 (1970). These authors showed that the mechanical properties of the nonfaceted transparent ''plastic'' organic crystals are similar to those of metals of the same crystal structure (fcc, in our case) at the same reduced temperature (absolute temperature divided by the melting temperature).
[11] S. de Cheveigné, C. Guthmann, and M.-M. Lebrun, J. Phys. (Paris) **47**, 2095 (1986). Also see M.-M. Lebrun, Thesis, Université Paris 7, 1987.
[12] S. Akamatsu, G. Faivre, and T. Ihle, Phys. Rev. E **51**, 4751 (1995).
[13] S. Akamatsu and G. Faivre, Phys. Rev. E **58**, 3302 (1998).
[14] M. Ginibre, S. Akamatsu, and G. Faivre, Phys. Rev. E **56**, 780 (1997).
[15] D.P. Woodruff, *The Solid-Liquid Interface* (Cambridge University Press, Cambridge, 1973). Also see R. Kikuchi and J.W. Cahn, Phys. Rev. **21**, 1893 (1985).
[16] P. Kopczynski, W.-J. Rappel, and A. Karma, Phys. Rev. E **55**, 1282 (1997).
[17] H. Jamgotchian, R. Trivedi, and B. Billia, Phys. Rev. E **47**, 4313 (1993).
[18] J. Mergy, G. Faivre, C. Guthmann, and R. Mellet, J. Cryst. Growth **134**, 353 (1993).
[19] S. Akamatsu and G. Faivre, J. Phys. I **6**, 5037 (1996).
[20] Grain coarsening involves the whole GB network of the solid. The lateral displacements of the GB grooves that we observe along the front are part of this process. They occur during directional solidification as well as at rest.
[21] W.A. Tiller, K.A. Jackson, J.W. Rutter, and B. Chalmers, Acta Metall. **1**, 428 (1953).
[22] For an introduction to the theory of the Mullins-Sekerka bifurcation, see B. Caroli, C. Caroli and B. Roulet, in *Solids Far from Equilibrium*, edited by C. Godrèche (Cambridge University Press, Cambridge, 1992).
[23] R.J. Schaefer, M.E. Glicksman, and J.D. Ayers, Philos. Mag. **32**, 725 (1975).
[24] M. Gündüz and J.D. Hunt, Acta Metall. **33**, 1651 (1985).
[25] K.A. Jackson, Philos. Mag. **7**, 1615 (1962).
[26] B. Chalmers, *Principles of Solidification* (Krieger, Huntington, NY, 1977).
[27] S. Akamatsu, S. Moulinet, and G. Faivre, Metall. Mater. Trans. A **32**, 2039 (2001).
[28] E. Billig, Proc. R. Soc. London, Ser. A **235**, 37 (1956).
[29] An externally applied stress can provoke an Asaro-Tiller-Grinfeld instability of the front in a dislocation-free crystal [see I. Cantat, K. Kassner, C. Misbah and H. Müller-Krumbhaar, Phys. Rev. E **58**, 6027 (1998)]. The present study suggests that, in a ductile crystal, such a stress would simply result in an enhancement of the dynamical polygonization.
[30] J.D. Verhoeven and E.D. Gibson, J. Cryst. Growth **11**, 39 (1971).
[31] K.A. Jackson and J.D. Hunt, Trans. AIME **236**, 1129 (1966).
[32] J.S. Langer, Phys. Rev. Lett. **44**, 1023 (1980).
[33] W. Datye and J.S. Langer, Phys. Rev. B **24**, 4155 (1981).
[34] M. Plapp and A. Karma, Phys. Rev. E **60**, 6865 (1999).